Poster presentation | Poster session

Poster Session

Thu. Jul 18, 2024 4:30 PM - 6:30 PM Room P

[PO-12] Fluid-Structure Interaction and Dynamic Mode Decomposition Analysis of a Nonslender Cropped Delta Wing in Transonic Regime

*Sheila Chica Francisco Langa[1], Yusuke Takahashi[1] （1. Hokkaido University）

Keywords: Fluid-structure interaction, Limit cycle oscillations, Dynamic mode decomposition, Transonic flow

Fluid-Structure Interaction and Dynamic Mode Decomposition Analysis of a Nonslender Cropped Delta Wing in Transonic Regime

Sheila C. F. Langa* and Yusuke Takahashi*
Corresponding author: sheilachicafrancisco.langa.b0@elms.hokudai.ac.jp
* Space Transportation Systems Lab., Division of Mechanical and Space Engineering,
Hokkaido University, Kita 13 Nishi 8, Kita-ku, Sapporo, Hokkaido, 060-8628, Japan

Abstract: Nonlinear transonic aeroelastic phenomena such as flutter and limit cycle oscillations (LCO) on thin plate delta wings remain uncertain, posing a risk to the usage of delta wings in aerospace engineering applications. Thus, investigations that provide insight into the cause and/or mitigation mechanisms of such nonlinearities are crucial. This study aims to analyze the transonic aeroelastic flutter and LCO behavior of a nonslender cropped delta wing, using a Fluid-Structure Interaction (FSI) model. The FSI analysis was performed using the high-fidelity fluid solver SU2, the structural solver CalculiX, and preCICE as the coupling library, thus ensuring an open-source software (OSS) framework. Eigenfrequency results were found to be in good agreement with the experimental data and a Fast-Fourier Transform (FFT) analysis was performed to obtain the LCO frequencies and displacements. When compared to the experiment and other numerical data, results showed a constant frequency range to which a Dynamic Mode Decomposition (DMD) approach was used. In contrast with the FSI results, the DMD analysis indicated an increase in the LCO frequency, thus optimizing the FSI model.

Keywords: Fluid-structure interaction, Limit cycle oscillations, Cropped delta wing, Dynamic mode decomposition, Transonic flow

1 Introduction

Aeroelasticity, a multidisciplinary field comprising the interaction of inertial, elastic, and aerodynamic forces, remains a relevant and indispensable research area. This is not only due to the increase in demand for highly maneuverable and flexible aircraft, but also because certain aeroelastic phenomena are destructive and pose a risk [1] to aircraft operation. Such is the case of flutter, which is defined as a self-induced oscillatory instability [2] that can lead to structural failure [3, 4]. When observed in either subsonic or supersonic flow, flutter can be analyzed using linear theories [5]. However, when it occurs in the transonic regime, linear theories fail [6] to capture all of the complex aeroelastic effects due to the inherent nonuniformities and nonlinearities of the flow [7]. One nonlinear behavior of interest is denoted as a limit-cycle oscillation (LCO). Classified as flutter with a constant amplitude, LCOs can be benign when they occur beyond the flutter boundary and become stable under small disturbances, or malign when they occur beyond and below the flutter boundary and become unstable under small disturbances [6]. The varied reasons behind the nonlinear flutter and LCO occurrence are intriguing and call for more research in the field. Generally, most causes have been attributed to nonlinear aerodynamic phenomena such as the occurrence of shock waves and flow separation. However, nonlinear structural effects such as freeplay, stiffness, internal damping, material nonlinearities, and geometric plate nonlinearities have been found to play a considerable role in the occurrence of LCOs [3, 8, 9].

A way to confirm this behavior is by performing experiments, but it is very challenging to reproduce accurate results concerning the flow and structure conditions due to the scaling law [1]. This explains the necessity to model the aeroelastic system in a computationally coupled approach, where the fluid, solid, and their respective interaction are taken into consideration. Such a method is denoted as fluid-structure interaction (FSI), and when properly used, it is capable to capture nonlinearities such as LCO in an accurate manner. Analyzing an aeroelastic model using FSI comprises a lot of challenges and difficulties coming from the multi-physics nature of the flow [10, 11]. Usually, two main methods are used to tackle coupled analysis, namely monolithic and partitioned approaches. While the monolithic approach consists of solving the problem in a unified manner where both the solid and the fluid are discretized simultaneously [12], the partitioned approach is based on the discretization of each in a separate and

successive manner [13, 14]. Monolithic approaches have been considered more robust than partitioned methods, but the complexity in discretizing a new implicit model and the limitation in manpower for programming make it a rather unsuitable method to solve large-scale problems [15, 14, 10]. Thus, the partitioned approach is a viable alternative as it offers a reusable and flexible tool where each of the independent solvers can be coupled together and even replaced easily without much change in the original codes. One issue with the partitioned approach is that the data needs to be properly communicated and mapped at the fluid-solid interface [16]. Recently, preCICE, a highly sophisticated open-source coupling library that is capable of providing data communication and data mapping between different solvers has been developed [17]. preCICE enables a black-box partitioned coupling method by means of adapters that facilitate the switching between various solvers, thus making it a very flexible and advantageous solution [18].

In this study, the nonlinear aeroelastic flutter and LCO mechanism will be analyzed through a partitioned FSI model consisting of preCICE as the coupling library, SU2 as the fluid solver, and CaluliX as the structural solver. The object of the research is the nonslender delta wing experimented by Schairer and Hand [19] which is prone to LCO phenomena. This wing was first computationally analyzed by Gordnier and Melville using a linear structural model with full Navier-Stokes [20, 21] where the occurrence of LCO was due to the leading edge vortices and shockwaves formed on the wing. When Gordnier analyzed the model using a nonlinear structural model, however, the LCO occurrence was due to the stiffness of the membrane plate due to the von-Karman model applied to it [22]. The nonlinear model was enhanced in an Euler-based study by Attar and Gordnier [23] where it was shown that the LCO was due to the geometric plate nonlinearities, although vortex formation was seen for higher dynamic pressures. Terashima and Ono [24] compared linear and nonlinear models on the wing using a Navier-Stokes model. They observed that vortices were formed in the linear model, but the geometrical nonlinearities caused a suppression in the deformation in the nonlinear model and suggested the use of turbulence modeling and good grid quality. Peng and Han [9] added the importance of material nonlinearities in a Euler-based nonlinear model. A recent paper from Ye e al. [25] analyzed the effect of angle of attack and noted that the nonlinear behavior of the wing differed at different angles of attack. The above studies prove the high sensitivity of the nonslender delta wing and thus indicate the need for further analysis of the same. The above studies mainly use Euler and Navier-Stokes models. Additionally a combination of structured and unstructured meshes are used. The current work, however, aims to use a fully open-source software (OSS) framework in Navier-Stokes and RANS modeling. The OSS model is chosen due to its high degree of freedom [1]. Two main general approaches will be presented on the analysis of the cropped delta wing, namely the study of the geometrically linear model, and the geometrically nonlinear model. For the nonlinear case, the effect of turbulence modeling, the effect of small angles of attack, and the model optimization using a data-driven dynamic mode decomposition (DMD) model will be presented. Results will be compared with the experimental data [19], and numerical studies [9, 23, 24] to ensure the validity of the proposed FSI and DMD models.

2   Computational Model

The current model comprises SU2 as the finite-volume-based fluid solver based on unstructured meshes [26], CalculiX as the finite-element-based solver for structural dynamics [27], and preCICE as the coupling library [18] between the two in an FSI approach. The data is transferred between the solvers through adapters. The FSI results will then be optimized through a DMD model. This section aims to describe the models and the algorithms used in the analysis.

2.1   Analytical Object

The analytical object of the FSI study is the nonslender cropped delta-wing with a 47.8° leading-edge sweep and -8.7° trailing edge-sweep placed in freestream transonic flow. The geometrical specifications of the model can be seen in Figure 1. The root length is 0.29845 m, the semi-span length is of 0.232 m, and the wing thickness is of 0.000889 m. The wing is considered to have a zero-angle of attack unless stated otherwise. Experimentally, the wing was considered to be of cold-rolled steel. In this model however, the wing material is set to be steel in a comparative approach to the work of Peng and Han [9].
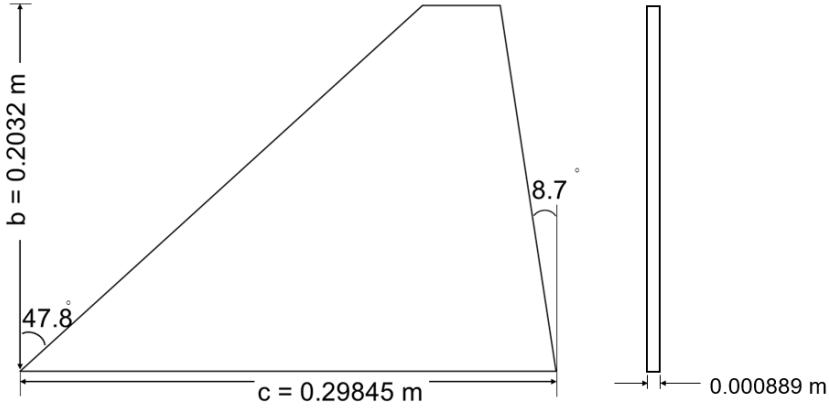
Figure 1: Cropped delta wing dimensions

2.2 Aerodynamic Solver

The fluid solver used in this numerical investigation is the unstructured-mesh fluid solver, SU2 [26]. The governing equations consist of the compressible Navier-Stokes (NS), and the compressible Reynolds-Averaged Navier-Stokes (RANS), both consisting of the momentum, total energy, and total density conservation laws. The NS and RANS were both discretized using the finite volume method. The ideal gas law and equation of state are included in the governing equations.

The thermodynamic properties of the ideal gas are the same as those of standard air. Two viscosity models are used in the current study for comparative analysis as done in the previous study [28]. The NS cases use the Sutherland viscosity model and the freestream Mach number, temperature, and velocity are kept fixed for simplicity. The RANS case on the other hand evaluates the viscosity through a constant viscosity model and all the parameters change per case. A Prandtl number of 0.72 is used for this analysis. For the RANS computations, Spalart-Allmaras turbulence modeling is considered. The evaluation of the advection term is done with the Jameson Schmidt Turkel (JST) scheme [29], and the spatial gradients are computed from the Green-Gauss technique. The unsteady state computations were handled by an implicit dual-time stepping time integration mechanism based on the 2nd order backward difference. For the inner iterations, a global time stepping approach is used. The solution method for the coefficient matrix is performed by the FGMRES method with the lower-upper symmetric Gauss-Seidel (LU-SGS) method incorporated into it for preprocessing. The SU2 version used for the current analysis is 7.5.0 with preCICE adapter installed, which enables data in unstructured format and provides high flexibility. The parallel computation was done using the message passing interface (MPI) and the domain decomposition method. The domain mode decomposition was performed using the standard parallel method for flow simulations on large scale computers, PARMETIS [30]. The grid deformation mechanism was implemented to ensure a stable deformation of the computational grids.

2.3 Structural Solver

The finite-element open-source structural solver CalculiX is used in this study [27]. The nonslender cropped delta wing was modeled as a three-dimensional object. Linear and isotropic material properties were considered. The computation of the structural dynamics equations was done through the principle of virtual work. Under the assumption that the model has no temperature changes, the equilibrium of momentum for the displacement field was obtained. The discretization of the governing equation is done from small elements and consisted of the element stiffness matrix, the element mass matrix, the element displacement, and the element load vector. The element mass matrix was computed by using the shape function incorporated into the formulation of the element stiffness matrix. The mass matrix, the load vector, and the stiffness equation were obtained by the definition of a displacement load vector. The Gauss-Legendre quadrature with the α-method [31] is used to solve the stiffness equation. The algorithm had a second-order accuracy and showed an unconditionally stable solution when $\alpha \in [-1/3, 0]$.

Calculix 2.20 with the preCICE adapter installed was used for the analysis model presented here. Both linear and geometrically nonlinear models were considered.

2.4   Coupling Method

The current numerical study uses a partitioned coupling method through the preCICE coupling library. The fluid and the solid counterparts are separately solved and coupled at the fluid-solid interface. While the fluid solver transmits force data and receives displacement data from the solid solver, the solid solver transmits displacement data and receives force data from the fluid solver. The computational grids are not necessarily the same at the interface. Even so, preCICE enables an appropriate data mapping interpolation at the coupling interface using the nearest-neighbor approach. Finally, the continuity and equilibrium conditions are satisfied through the implementation of a parallel-implicit scheme on the coupling boundary. The coupling algorithm is represented by Figure 2 [1].
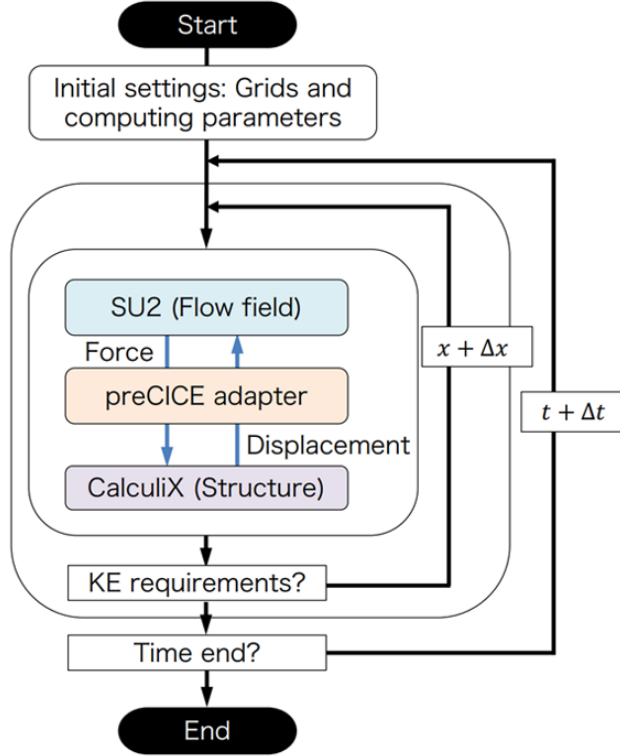

Figure 2: Flowchart of the coupling method using an implicit scheme. In the inner loop, x represents the boundary variables such as displacement and force that are transfered between the solvers, and t in the outer loop shows the time. Kinematical Equilibrium "KE" requirements are satisfied at the interface [1]

2.5   Computational Conditions

The material specifications of the cropped delta wing are considered to be uniform and using steel material properties with Young's Modulus of 200 GPa, Poisson's ratio of 0.3 and density of 7,850 kg/m^3, which are similar to the cold-rolled steel properties used in the experiment as seen in Table 1.

Table 1: Material properties comparison

Material	E (GPa)	v	ρ (kg/m^3)
Cold-rolled steel	206	0.25	7833
Steel	200	0.3	7850

Differently from the numerical computations to be compared with, which use a combination of structured and unstructured grids, the current model is based on fully unstructured grids. The structural grid used in this study is composed of 122,626 nodes as used in the previous work on the same wing [28], and the fluid mesh has 4,502,142 cells. The aerodynamic grid is refined using an inner domain and T-Rex layer extrusions to capture the phenomena near the wing. Both the structural and fluid grids can be seen in Figure 3(a) and Figure 3(b) respectively. For all scenarios, the freestream conditions are evaluated from the isentropic process. No pressure gradients and no-slip conditions to the normal direction at the
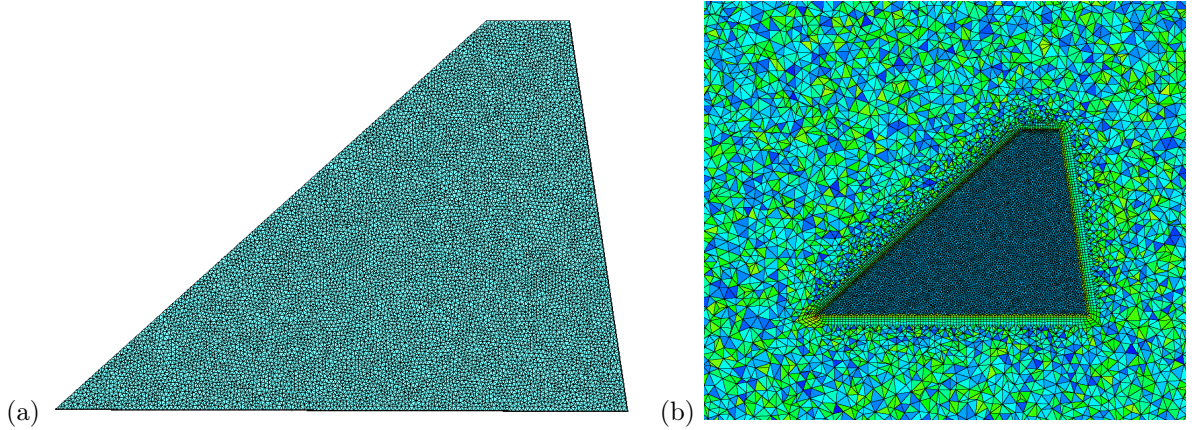
Figure 3: Computational grids: (a) solid grid (b) fluid grid

wing surface are assumed. All of the wing surfaces are modeled as coupled interfaces. The analysis is performed through a change of dynamic pressures. In this study, only three dynamic pressure cases will be considered namely 20.54 kPa (2.98 psi), 21,78 kPa (3.16 psi), and 22.96 kPa (3.33 psi). The Reynolds number has an order of magnitude of 10^6, and a Reynolds length of 0.298 m is considered.

The meshes are constrained as fixed at the bottom surface while all other surfaces are able to move freely. The transonic Mach number ranged from 0.878 to 0.876 for the nonlinear computations and was kept at 0.9 for the linear cases. For all of the linear NS computations the angle of attack is set to zero, and the nonlinear RANS computations show a variation of angle of attack in small ranges namely $0°$, $0.1°$, and $1°$ for a comparative analysis. Additionally, turbulence modeling is used only in the RANS case, with the Spalart-Allmaras (SA) method.

2.6   Mode Decomposition and Reconstruction Scheme

The computational results of the FSI simulation will be analyzed by an open-source data-driven dynamic-mode decomposition (DMD) software called Revun [32]. The DMD approach in Revun consists of reading .vtu or .vtk data formats and predicting the highest modes using a mode-sensing technique.The data is read from the structural displacement, where the generated .frd file by CalculiX is first decomposed into .vtk formats and then analyzed. The data is reconstructed, and eigenvalue modes are also found and compared with the FSI data. The greedy algorithm is used in the DMD code as seen in Figure 4.

Algorithm 1 Mode sensing using Greedy algorithm

Input: d: displacement reconstructed in mode set $\mathbb{M}$, d_{FSI}:
   displacement by FSI
Output: d_{R}: displacement accumulated
 1: Initialize solution and index set: $d_{\text{R}} = 0$, $\mathbb{J} = \emptyset$
 2: **while** not TerminationCondition: $\|d_{\text{FSI}} - d_{\text{R}}\| \leq \varepsilon$ **do**
 3:    Initialize the residual: $F = HugeValue$
 4:    **for** $i \leftarrow 1 \rightarrow |\mathbb{M}|$ **do**
 5:       **if** $i \notin \mathbb{J}$ **then**
 6:          Calculate the residual: $F_i = \|d_{\text{FSI}} - d_i\|$
 7:       **end if**
 8:    **end for**
 9:    Select index that minimizes the residual: $I = \underset{i \in \mathbb{M}}{\arg\min} \, F_i$
10:    Add the index: $\mathbb{J} \leftarrow I$
11:    Update the solution: $d_{\text{R}} \leftarrow d_I$
12: **end while**
13: **return** Solution

Figure 4: Mode sensing using the greedy algorithm employed in Revun [32]

3   Results and Discussions

In this section, we start by outlining the results of the eigenfrequency analysis, followed by a discussion of the FSI model of the wing in transonic flow. Finally, the chosen optimization technique using the DMD approach is discussed and compared.

3.1   Eigenfrequency Analysis

The natural frequencies of the current model were analyzed through the finite element solver CalculiX. The eigenfrequency analysis was performed by solving the following equation:

$$Kx = \lambda Mx \tag{1}$$

Where K represents the overall stiffness matrix, M represents the overall mass matrix, λ is the eigenvalue, and x is the eigenvector. The comparison of the modal analysis to the experiment are found in Table 2.

Table 2: Natural vibration modes comparison

Case	Mode 1	Mode 2	Mode 3
Experiment [19]	26.7 Hz	88.2 Hz	131.8 Hz
Peng and Han [9]	26.5 Hz	87.7 Hz	131.9 Hz
Simulation	26.46 Hz	87.59 Hz	131.94 Hz

The modal frequency results are much closer to those of the numerical results by Peng and Han [9] than the experimental ones, as is to be expected. Modes 1 and 3 are much closer to the experiment than mode 2. Nevertheless, the dominant motions of the wing were consistent with those of the experiment with first bending for the first mode, first torsion for the second mode, and second bending for the third mode. These can be seen in Figure 5. Thus, the validity of the current structural model was ensured.
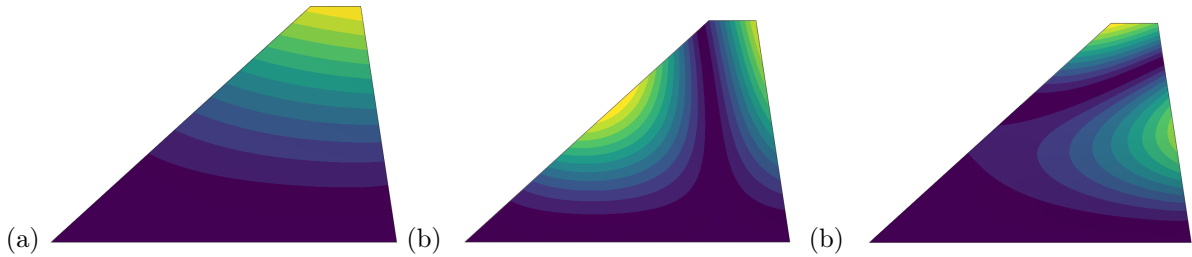

(a)   (b)   (b)

Figure 5: Vibration modes: (a) first mode, (b) second mode, (c) third mode

3.2   Geometrically Linear Model

A geometrically linear model was analyzed in order to validate the current FSI model toward capturing the aeroelastic behavior of the wing. This was mainly conducted due to the fact that it has been observed that the reason behind the occurrence of the nonlinear LCO phenomena differs greatly [20, 21, 24] according to the structural model chosen, thus proving the sensitivity of the analytical object of this study. Results are shown on the 20.54 kPa case, with a Reynolds number of 2.57E6.

3.2.1   Vortex and Shockwave Formation

In the computations by Gordnier and Melville [20, 21], it was observed that the cause of the LCO was on the unsteady vortex formation on the wing surface which caused a 180 degree out of phase motion of the delta wing. They further noted that the vortex acted as an aerodynamic spring, which caused the wing to show LCOs. Additionally, the formation of shockwaves between the upstroke and downstroke of the wing was observed in their results. In their computations, however, the angle of attack was increased, and it was then, that such a roll-up vortex phenomenon was observed.

Differently from their setup, the linear numerical model presented in this study has a zero angle of attack. Nevertheless, the aeroelastic phenomena observed from the results show a very similar outcome.
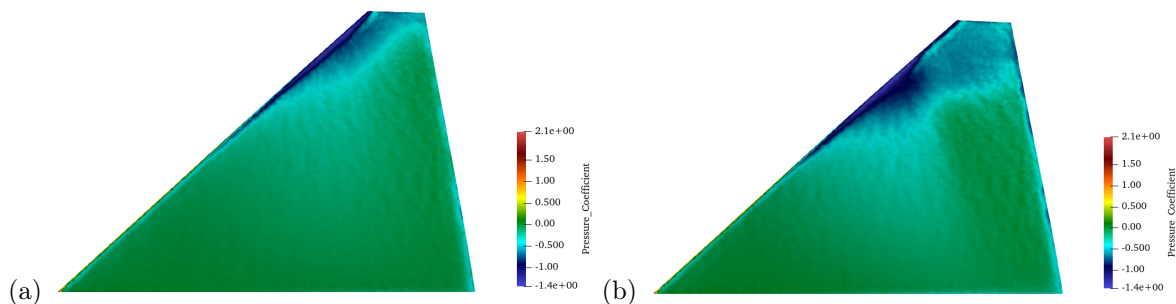
Figure 6: Pressure coefficient on the wing surface: (a) weak vortex footprint, (b) double shock

Figure 6 shows that the current FSI model was able to capture the unsteady aeroelastic phenomena, as leading-edge vortices were formed on the wing surface. Figure 6(a) shows a weak vortex footprint, whereas 6(b) shows a double shock in the upstroke motion of the wing. The shockwave can also be seen at the surface of Figure 6(b). A better visualization is provided in Figure 7, since not only the downstroke and downstroke motions are outlined, but also the occurrence of dual shockwaves can be seen in (b). This result reveals that the linear model used in this work is capable of showing vortex behavior and shockwave formation at a zero angle of attack, thus differentiating it from previous research.
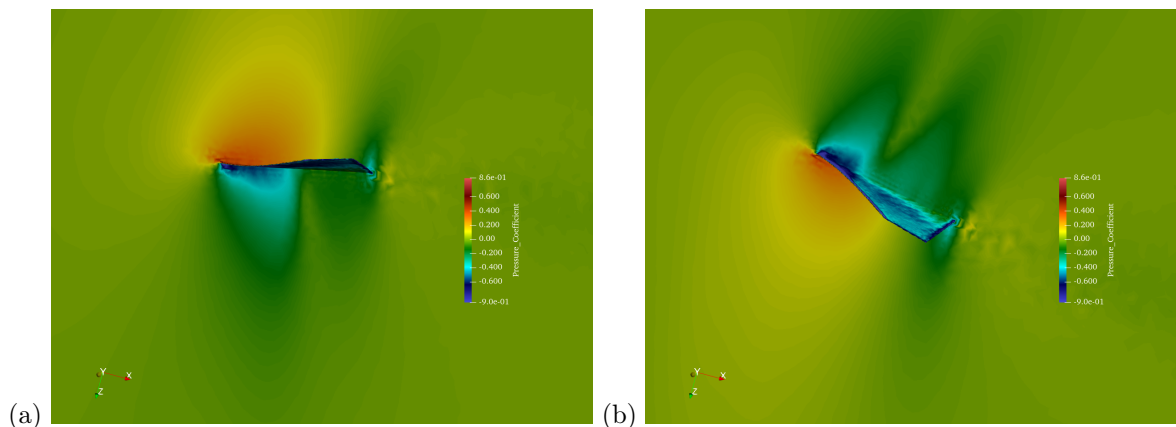
Figure 7: Pressure coefficient of the flow: (a) single shock, (b) dual shock

3.2.2 Wing Deformation

To analyze the results from the large-deformation observed in the linear model, a comparison to the work of Terashima and Ono [24] is shown in Figure 8.
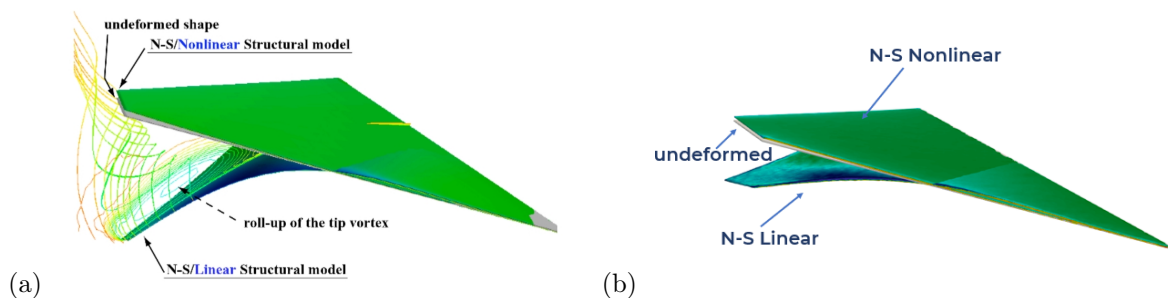

Figure 8: Large-deformation qualitative comparison: (a) linear and nonlinear model as computed by Terashima and Ono [24], (b) linear and nonlinear models computed in current simulation

A Fast-Fourier Transform (FFT) using the displacement data was performed to obtain the LCO frequencies and LCO amplitudes of the wing. From a qualitative perspective, it is clear that the presented linear FSI model shows a much lower LCO amplitude in comparison. This is even more pronounced,

as in the case of Figure 8(a) the dynamic pressure is 19.16 kPa as compared to 20.54 kPa used in (b). Since the LCO amplitude should increase as we increase the dynamic pressure, case (b) should show a larger amplitude than (a). The fact that the opposite is seen denotes that the current model underpredicts the LCO amplitude of the nonslender cropped delta wing. Nevertheless, this does not erase the fact that the difference in LCO amplitude between the linear and nonlinear models is extensive. For comparison, a Navier-Stokes nonlinear computation including geometrical plate nonlinearities under the same computational conditions was performed and the respective results can be seen in Figure 9 below. Here, the LCO frequency for the linear case is 55.9 Hz as compared to 51.9 Hz in the nonlinear case.
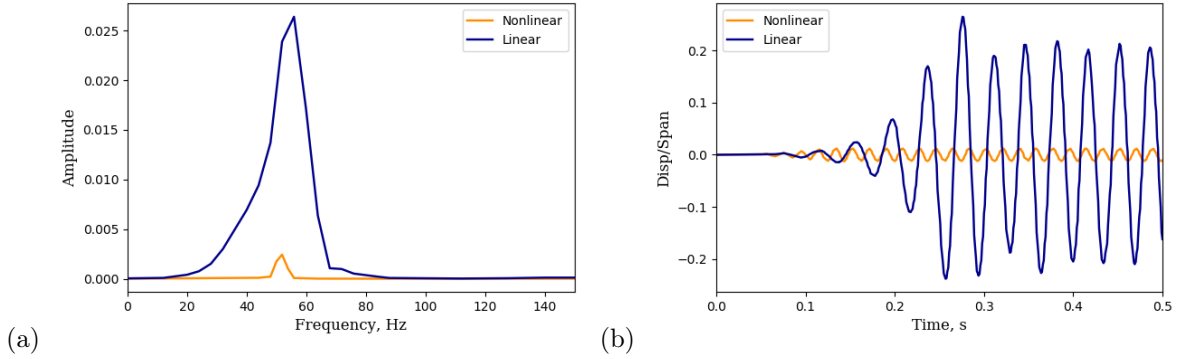

Figure 9: Linear and nonlinear comparison: (a) frequency, (b) displacement

3.3 Geometrically Nonlinear Model

A geometrically nonlinear model was also analyzed in order to validate the current FSI model toward capturing the aeroelastic behavior of the wing. The effect of turbulence modeling on the proposed numerical study was performed by comparing the NS solution to the modified RANS-SA model used. Both cases use the same computational domain, the same freestream parameters, but differ in the governing equation. An initial comparison with a fixed zero angle of attack can be seen in Figure 10. The analysis results show that there is a slight difference in LCO amplitude, to the fact that the NS case shows a slightly higher LCO displacement in comparison to the RANS-SA model. Yet, from the transition from (a) to (c) it can be said that as the dynamic pressure increases, the difference in LCO amplitude between the two models decreases.
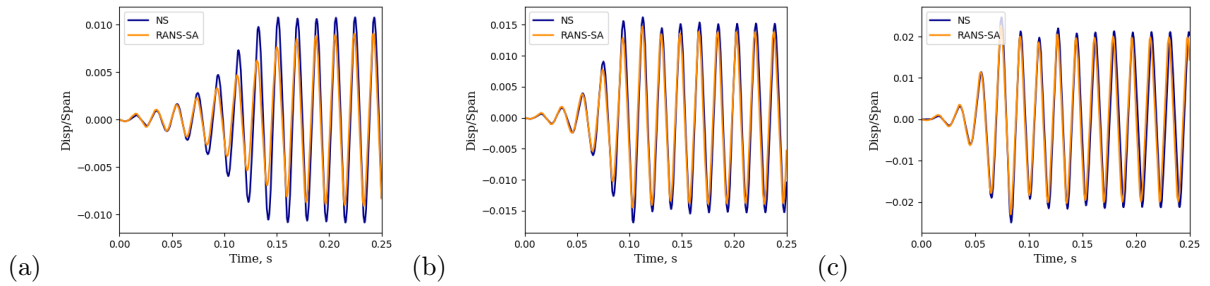

Figure 10: NS vs RANS-SA: (a) 20.54 kPa, (b) 21.72 kPa, (c) 22.96 kPa

The LCO displacement results were then compared to the experiment [19] and other numerical studies [23, 9]. The lower LCO amplitude is confirmed as can be seen in Figure 11. This is to be expected, since the model used in this simulation uses a Navier-Stokes-based fluid model, whereas the studies in comparison use an Euler-based fluid model. As concluded in the computational study of Gordnier [22], Euler equations showed a higher LCO amplitude and smaller LCO frequency than the NS model. This suggests the need to analyze the current wing model using Euler equations, as the turbulence modeling did not increase the amplitude, but inversely decreased it in comparison to the case with no turbulence modeling included.
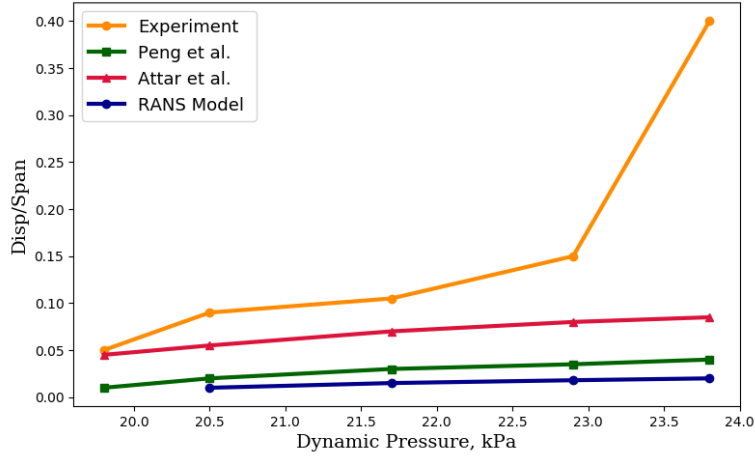
Figure 11: LCO displacement comparison

3.3.1 Effect of Angle of Attack

The angle of attack was modified in the RANS-SA case. Here, results are shown for the 20.54 kPa case for a comparative analysis. From the outputs in Figure 12, it was seen that the model had a stable LCO in the case of angle of attack set to 0°. At a slight increase from 0° to 0.1°, the LCO phenomena is still observed although at a very different behavior resembling the LCO phenomena at a larger dynamic pressure. When the angle of attack is raised to 1°, however, the wing no longer experiences LCO, but shows a stable flutter behavior. The results can be seen below, as it is confirmed that the change in angle of attack changes the LCO behavior in terms of displacement.
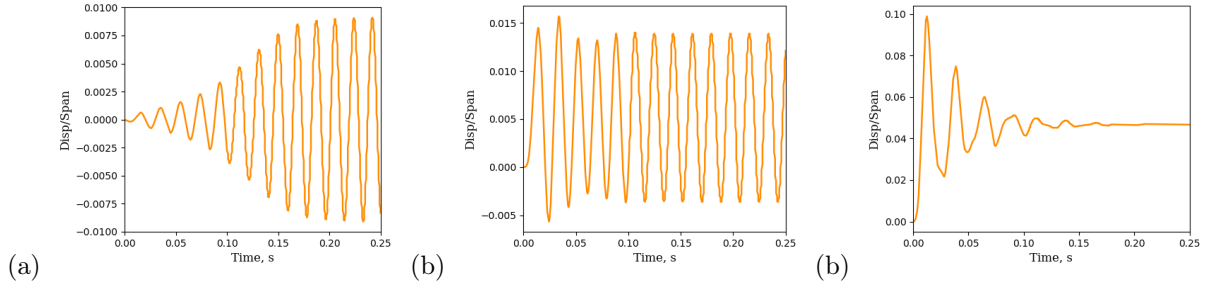

Figure 12: Angle of attack comparison: (a) 0°, (b) 0.1°, (c) 1.0°

3.4 DMD Analysis

Similar to the conclusion in the previous numerical study in [28], the current FSI model showed a constant frequency range in the output. This is an unusual phenomena as the model should not only experience an increase in LCO amplitude but also in frequency as the dynamic pressure is increased. Such an increase was only seen from 20.54 to 21.72 kPa, but the frequency remained the same from 21.72 to 22.96 kPa.

In order to understand this phenomenon, the DMD analysis was performed using the open-source software, Revun [32], thus ensuring a fully OSS approach from the FSI to the optimization model. The analysis consisted of the displacement data written by CalculiX in which the file was converted to single .vtk formats to represent each time step. The current model had 2.5E-4 time steps that run for a time range of 0.25s, thus the displacement data was composed of 1000 files. From these, the DMD analysis was performed from steps 100 to 1000, using the same time step of 2.5E-4. The reconstructed results showed that the wing was governed by the first bending mode and the comparison of the reconstructed data and the Mach distribution of the FSI result can be seen in Figure 13. The mode sensing technique was applied to find the leading modes in the cropped delta wing. Results revealed no constant frequency range in different dynamic pressures as seen in Figure 14, thus showing that the DMD model optimizes the FSI results. The overprediction of the LCO frequency however, calls for an in-depth analysis of the current model and what other reasons may influence it apart from the governing equations.
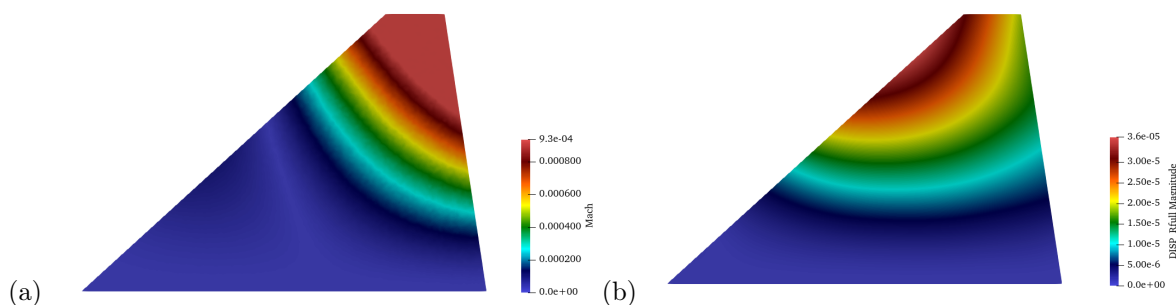
Figure 13: Surface flow comparison: (a) FSI model, (b) DMD reconstructed model
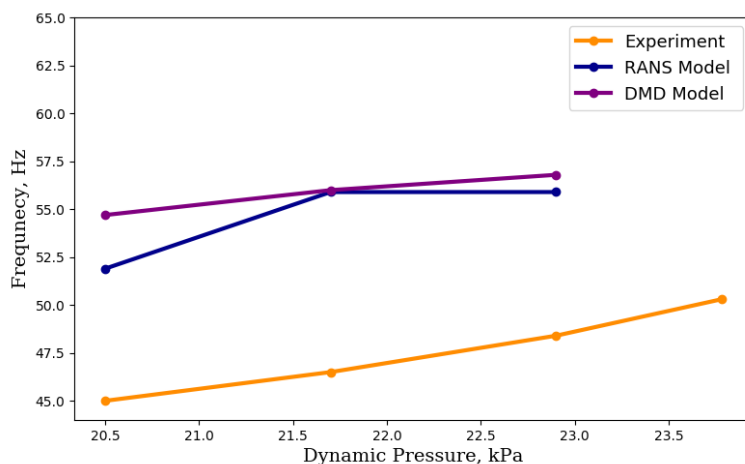

Figure 14: Comparison between primary frequencies detected by DMD with FSI results and experiment

4   Conclusions

In this study, the nonlinear aeroelastic flutter and LCO of a nonslender cropped delta wing was analyzed in a coupled manner using a fully open-source framework. Two analysis models were proposed namely geometrically linear and nonlinear, in which both Navier-Stokes and RANS modeling were presented. The model was then compared to the experiment and other numerical studies on the same cropped delta wing. It was seen that the presented FSI model captured vortex and shockwave formation in the linear model at a zero angle of attack. Thus, showing a unique feature of the model's ability to observe complex aeroelastic phenomena even without the increase of angle of attack. The nonlinear case revealed that RANS-SA produced a smaller LCO amplitude than NS. When the angle of attack was changed, the frequency remained the same but the LCO amplitude differed. The constant frequency region was observed over a range of dynamic pressures which called for an optimization of the model. The optimization method chosen, DMD, proved to enhance the FSI results as no constant frequency range was observed. Despite this enhancement, the NS model showed an overprediction of the LCO frequencies which calls for future optimizations in the FSI model itself for lower frequency values and higher amplitudes, such as the use of Euler equations in the governing models.

Acknowledgements

References

[1] Yusuke Takahashi. Large-deformation limit-cycle oscillation of a delta wing using fluid-structure interaction analysis at transonic speed. *Available at SSRN 4135441*, 2022.

[2] WJ Duncan. Flutter and stability. *The Aeronautical Journal*, 53(462):529–557, 1949.

[3] Earl H Dowell. *A modern course in aeroelasticity*, volume 264. Springer Nature, 2021.

[4] Raymond L Bisplinghoff, Holt Ashley, and Robert L Halfman. *Aeroelasticity*. Courier Corporation, 2013.

[5] Heinrich J Ramm. *Fluid dynamics for the study of transonic flow*. Number 23. Oxford University Press, USA, 1990.

[6] Charles M Denegri Jr and Michael R Johnson. Limit cycle oscillation prediction using artificial neural networks. *Journal of guidance, control, and dynamics*, 24(5):887–895, 2001.

[7] Oddvar O Bendiksen. Review of unsteady transonic aerodynamics: Theory and applications. *Progress in Aerospace Sciences*, 47(2):135–167, 2011.

[8] Deman Tang, James K Henry, and Earl H Dowell. Limit cycle oscillations of delta wing models in low subsonic flow. *AIAA journal*, 37(11):1355–1362, 1999.

[9] Cui Peng and Jinglong Han. Numerical investigation of the effects of structural geometric and material nonlinearities on limit-cycle oscillation of a cropped delta wing. *Journal of Fluids and Structures*, 27(4):611–622, 2011.

[10] Bernhard Gatzhammer. Efficient and flexible partitioned simulation of fluid-structure interactions. 2015.

[11] Friedrich-Karl Benra, Hans Josef Dohmen, Ji Pei, Sebastian Schuster, and Bo Wan. A comparison of one-way and two-way coupling methods for numerical analysis of fluid-structure interactions. *Journal of applied mathematics*, 2011(1):853560, 2011.

[12] Björn Hübner, Elmar Walhorn, and Dieter Dinkler. A monolithic approach to fluid-structure interaction using space-time elements. *Computer Methods in Applied Mechanics and Engineering*, 193:2087–2104, 06 2004.

[13] Th Dunne, Rolf Rannacher, and Th Richter. Numerical simulation of fluid-structure interaction based on monolithic variational formulations. *Fundamental trends in fluid-structure interaction*, pages 1–75, 2010.

[14] Serge Piperno. Explicit/implicit fluid/structure staggered procedures with a structural predictor and fluid subcycling for 2d inviscid aeroelastic simulations. *International journal for numerical methods in fluids*, 25(10):1207–1226, 1997.

[15] Hazel Andrew Boyle Jonathan Heil, Mathias. Solvers for large-displacement fluid–structure interaction problems: segregated versus monolithic approaches. *Comput. Mech*, 2007.

[16] Bernhard Gatzhammer, Miriam Mehl, and Tobias Neckel. A coupling environment for partitioned multiphysics simulations applied to fluid-structure interaction scenarios. *Procedia Computer Science*, 1(1):681–689, 2010.

[17] Miriam Mehl, Benjamin Uekermann, Hester Bijl, David Blom, Bernhard Gatzhammer, and Alexander Van Zuijlen. Parallel coupling numerics for partitioned fluid–structure interaction simulations. *Computers & Mathematics with Applications*, 71(4):869–891, 2016.

[18] Hans-Joachim Bungartz, Florian Lindner, Bernhard Gatzhammer, Miriam Mehl, Klaudius Scheufele, Alexander Shukaev, and Benjamin Uekermann. precice–a fully parallel library for multiphysics surface coupling. *Computers & Fluids*, 141:250–258, 2016.

[19] Edward T Schairer and Lawrence A Hand. Measurements of unsteady aeroelastic model deformation by stereo photogrammetry. *Journal of Aircraft*, 36(6):1033–1040, 1999.

[20] Raymond Gordnier and Reid Melville. Physical mechanisms for limit-cycle oscillations of a cropped delta wing. In *30th Fluid Dynamics Conference*, page 3796, 1999.

[21] Raymond E Gordnier and Reid B Melville. Numerical simulation of limit-cycle oscillations of a cropped delta wing using the full navier-stokes equations. *International Journal of Computational Fluid Dynamics*, 14(3):211–224, 2001.

[22] Raymond E Gordnier. Computation of limit-cycle oscillations of a delta wing. *Journal of Aircraft*, 40(6):1206–1208, 2003.

[23] Peter J Attar and Raymond E Gordnier. Aeroelastic prediction of the limit cycle oscillations of a cropped delta wing. *Journal of Fluids and Structures*, 22(1):45–58, 2006.

[24] Hiroshi Terashima and Kenji Ono. Transonic aeroelastic computations of a delta wing conguration with high fidelity equations. In *Computational Fluid Dynamics 2006: Proceedings of the Fourth International Conference on Computational Fluid Dynamics, ICCFD, Ghent, Belgium, 10-14 July*

2006, pages 843–848. Springer, 2009.

[25] Kun Ye, Mengbing Yang, Liuzhen Qin, Rongrong Xue, and Zhengyin Ye. Effects of structural geometric nonlinearities on the transonic aeroelastic characteristics of wing. *Aerospace Science and Technology*, 149:109161, 2024.

[26] Thomas D Economon, Francisco Palacios, Sean R Copeland, Trent W Lukaczyk, and Juan J Alonso. Su2: An open-source suite for multiphysics simulation and design. *Aiaa Journal*, 54(3):828–846, 2016.

[27] CalculiX - a free software three dimensional strucutral element program, howpublished = www.calculix.de. Accessed: 2024-06-29.

[28] Sheila CF Langa and Yusuke Takahashi. Fluid-structure interaction of a cropped delta wing in transonic regime. In = *Proceedings of the Conference on Computational Engineering and Science/* , volume 28, pages 749–753. , 2023.

[29] Antony Jameson. Origins and further development of the jameson–schmidt–turkel scheme. *AIAA Journal*, 55(5):1487–1510, 2017.

[30] George Karypis, Kirk Schloegel, and Vipin Kumar. Parmetis. *Parallel graph partitioning and sparse matrix ordering library. Version*, 2, 2003.

[31] Isidoro Miranda, Robert M Ferencz, and Thomas JR Hughes. An improved implicit-explicit time integration method for structural dynamics. *Earthquake engineering & structural dynamics*, 18(5):643–653, 1989.

[32] Dynamic mode decomposition script for VTK/VTU data, howpublished = https://github.com/ytakahashi3123/revun. Accessed: 2024-06-29.